



OPTIMAL LOCATION OF ACTION POTENTIAL GENERATION BASED ON ACTIVATION FUNCTION USING COMPUTATIONAL MODELLING

^{1,2,*}Enver SALKIM 

¹Mus Alparslan University, Department of Electronics and Automation, Mus, TÜRKİYE

²University College London (UCL), Department of Electronics and Electrical Engineering, London, UK

¹e.salkim@alparslan.edu.tr, ²e.salkim@ucl.ac.uk

Highlights

- Transcutaneous electrical nerve stimulation (TENS)
- Activation function (AF)
- Finite element simulation (FEM)
- Bio-computational modeling simulation
- Nerve action potential generation
- Extracellular electrical potential



OPTIMAL LOCATION OF ACTION POTENTIAL GENERATION BASED ON ACTIVATION FUNCTION USING COMPUTATIONAL MODELLING

^{1,2,*}Enver SALKIM 

¹Mus Alparslan University, Department of Electronics and Automation, Mus, TÜRKİYE

²University College London (UCL), Department of Electronics and Electrical Engineering, London, UK

¹e.salkim@alparslan.edu.tr, ²e.salkim@ucl.ac.uk

(Received: 20.01.2023; Accepted in Revised Form: 05.07.2023)

ABSTRACT: Transcutaneous electrical nerve stimulation is used to elevate health-related disorders. This technology is now an important therapeutic system for medical science. In this system, the electrical current pulse is applied over the skin through the inner layers via electrodes to activate excitable tissue layers. Activating other excitable tissue layers may cause discomfort. Thus, it is vital to design electrode configuration arrangements to activate the target anatomical layers without affecting the neighboring ones. A device for primary headaches showed mixed results. This may be related to the electrode position that requires higher stimulus current levels to activate target nerve fibers. This may stimulate neighboring nerve fibers which resulted in the discomfort of patients. A feasible solution is to identify the optimal electrode configuration based on the activation function which is the second derivative of the electric potential along an axon. This may guide to estimate of the possibility of action potential generation on the neural tissue layer using a specified electrode arrangement. In this study, the multilayered human head was developed based on MRI data set using pre and post-processing. Then multi-electrode arrangements were developed to examine the possible nerve activation location. Results showed that the nerve fibers were activated at the same location of the trajectory for the anodal and cathodal stimulation. This may be proof that the activation function can be used to define the optimal location of nerve activation. This may lead to lower thresholds for similar therapeutic benefits in transcutaneous electrical nerve stimulation with decreased power consumption.

Keywords: Action Potential, Activation Function, Extracellular Potential, Finite Element Simulation

1. INTRODUCTION

Transcutaneous electrical nerve stimulation (TENS) is a non-invasive therapy method. This alternative procedure is widely preferred for its non-invasiveness, ease of use, reusability, and reconfigurability [1]–[3]. By using the TENS method, the action potential is achieved by applying stimulus current levels to the excitable neural tissue layers over the skin using electrode arrangements [4], [5]. It is desired to activate target excitable tissue without activating other neural tissue in the vicinity. However, it may not be possible to achieve optimal stimulation as always. There are many factors that may affect the outcome. i) it may not be possible to control the transcutaneous delivery of charges which may lead to activating the excitable tissue nearby apart from the target neural tissue, ii) the relatively higher current levels may activate the neighboring excitable tissue which results in discomfort, iii) it has been shown that sensory nerve fibers may require lower current levels than motor nerve fibers. This may activate superficial pain nerve fibers which are not desired [1], [6], [7]. Consequently, it is required to apply a higher stimulus current when targeting deeper excitable tissue layers. This will, in turn, result in a large volume of the electrical potential distributions within the volume conductor. Also, using higher current levels may result in higher current density which may cause inflammations and skin burns [8], [9]. A neuromodulator for primary headaches showed mixed results. It has been shown that most users complain about discomfort, pain, and inflammation [10], [11]. This may be related to the higher stimulus current levels that are applied through the electrodes which may be caused to activate the pain sensory nerve fibers of neighboring neural elements. A feasible solution to reduce the required current levels by re-defining the location of the

*Corresponding Author: Enver SALKIM, e.salkim@ucl.ac.uk, e.salkim@alparslan.edu.tr

stimulation electrodes for optimal stimulation strategy. It has been shown that the activation function (AF) can be used to determine the possible place of the neural action potential generating based on given neuromodulator settings. This may lead to lower thresholds for similar therapeutic benefits in transcutaneous electrical nerve stimulation with decreased power consumption using appropriate simulation settings. It is not possible to analyze the location of the action potential generation using experimental methods due to possible risks. Computational modeling methods can be an appropriate alternative, and it has been used for many designing and optimization neuromodulators to analyze the impact of electrical stimulation on neural elements [4], [12], [13]. In this alternative method, the neural response to electrical stimulation is calculated using a finite element model (FEM). These computational FEM models are constructed based on a volume conductor model representing various anatomical structures and the electrodes by their respective electrical parameters (conductivity, dielectric permittivity) and appropriate boundary conditions. It has been shown that the possible location of the action potential generation can be predicted using AF for different neuroanatomical targets using such computational methods [14], [15]. Also, studies have shown that AF can be used for different simulation methods (e.g., magnetic simulation) [16] and invasive neuromodulation techniques including deep brain stimulation [17]. In this procedure, the electrical potential distributions were calculated then the response of the neural elements was calculated based on the second derivative of electrical potential using electrode settings.

In this study, the human head volume conductor based on various tissue layers was generated using FEM and TENS-based strategy to investigate the possible nerve activation location on the forehead. The human head's fundamental anatomical layers including skin, muscle, skull, and brain were constructed based on an adult magnetic resonance image (MRI) data set. The pre-process was applied to the MRI data set to identify tissue layers' grayscale and their boundary in MATLAB v.R2019 (MathWorks, Inc., Natick, MA, USA) as shown in Fig. 1 and 3. Then, each tissue layer was imported to COMSOL Multiphysics (COMSOL, Ltd, Cambridge, UK) to generate the complete human head model. The anatomical variation of the nerve was obtained from [18], [19] and the nerve model was generated based on Supraorbital (SON) and Supratrochlear (STN) nerve branches of the frontal nerve. The models were merged with the human head in COMSOL accordingly. The electrode configuration was generated in COMSOL and merged with the head model volume conductor to calculate AF using appropriate current settings as shown in Fig. 3. The electrical potential was simulated for a given electrode configuration with incremental steps on the forehead. The AF was calculated for both anodic and cathodic stimulation to define the optimal nerve fiber activation on the forehead.

2. MATERIAL AND METHODS

2.1 MRI Data Processing

The pre-process was applied to the MRI data set to generate a computational efficiency human head model. The multi-tissue layers and their relative coordinate points were derived from the MRI data set of the human head. This data set was obtained from [20] which is called MIDA. The MIDA model is a multimodal imaging-based detailed anatomical computer model of the human head and neck. The overall model includes 350 sagittal, 480 coronal, and 480 transverse planes of MRI slices. It is available in different voxel data formats (.nii, .mat, .raw) and the model spatial resolution (0.5 mm isotropic). The transverse MRI data and (.nii) voxel data format was performed in this study. To visualize and process the data, *NIFTI* (Neuroimaging Informatics Technology Initiative) and *ANALYZE* image tools were applied according to the required setting. It was noted that *load_nii* and *view_nii* functions were applied based on their library settings to visualize the MRI data set in three-dimensional (3D) in MATLAB. These functions were activated individually for each visualization and processing step. Different transverse human head slices were visualized in MATLAB as shown in Fig. 1. It was shown that the data constructed many slices and different ranges of gray-scale values. Thus, it is required to do image pre-processing to generate a computationally efficient model.

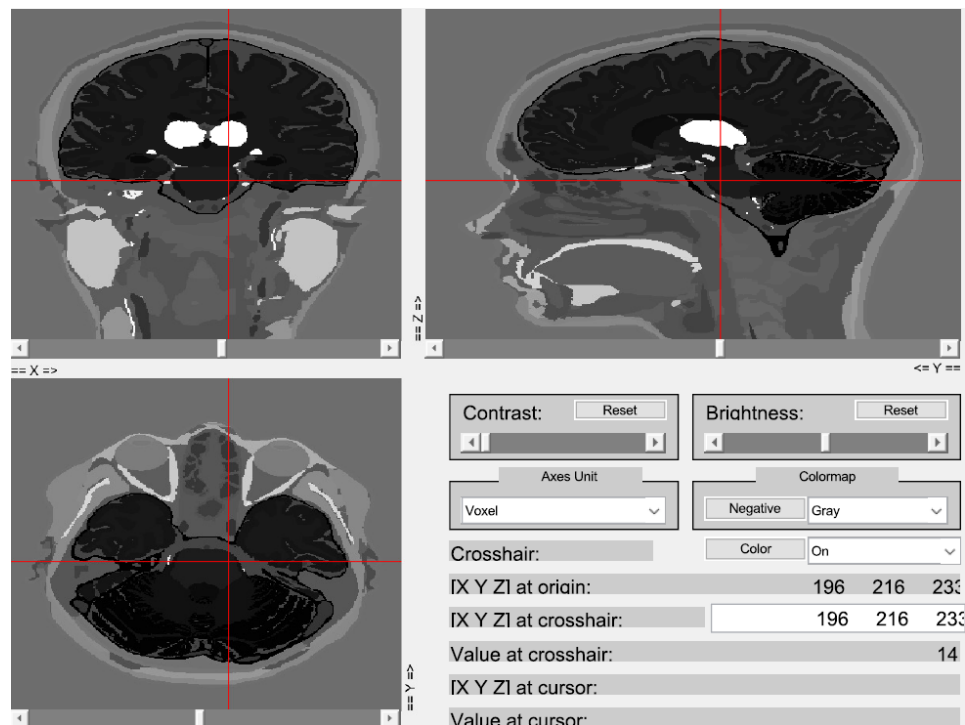


Figure 1. Visualization of the 3D MRI data set using required functions in MATLAB. It is shown that the data includes many slices and a large scale of the gray scale.

2.2 Volume Conductor Development

The pre-processing was applied to the MRI data set to generate an efficient and accurate human-head computational model. The 3D human head model was constructed from 30 transverse two-dimensional (2D) MRI image slices with minimum spacing, which was 5 mm, whilst maximum spacing was 12.5 mm. Each tissue layer's coordinate points were manually selected on the same MRI image to define contours. Then, the arc-length vector of the contours was defined with different amounts of denser points for each tissue layer in MATLAB. These denser points were interpolated with *Piecewise Cubic Hermite Interpolating Polynomial* (PCHIP) function to have more smooth contours in MATLAB.

The work plane (z coordinate) was defined for each smooth contour slice, according to image slice spacing in COMSOL Multiphysics. The related contour denser points were imported into COMSOL Multiphysics as an interpolation solid curve. To generate volume from two different work planes, the *loft function* in Design Module in COMSOL software was applied. To have a better meshed solid object, columns face partitioning was adjusted to apply *loft function* properly to the overall of the 30 transverse slices. The lofted profiles should be adjusted as a union after generating an individual tissue in 3D volume because the union function provides the user to control tissue (which could have intersections with each other) and add this tissue's electrical features manually to obtain simulation results. These steps are summarized in Fig. 2.

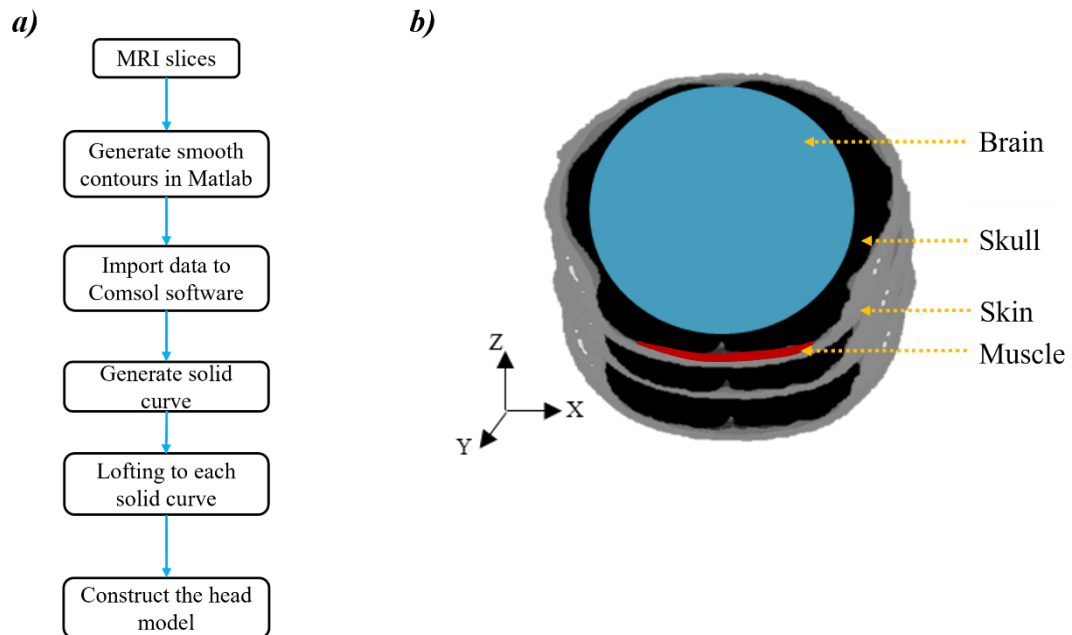


Figure 2. (a) Shows the process steps of generating the 3D CAD human head model. The smooth contours were generated using image processing filters then these were exported to COMSOL to generate 3D models. (b) shows the visualization of the smooth MRI data set. The image data was processed to generate the fundamental tissue layers including the brain, skull, muscle, and skin.

The current study volume model was composed of six tissue layers. These are, in turn, electrode patches, skin, nerve, muscle, skull, and the rest of the volume was assumed as a brain. These layers are represented in Fig. 2. The skin layer is built from 30 MRI slices, muscle volume was generated based on 10 slices, the skull was constructed from 27 slices, and the brain was assumed to be an ellipsoid shape due to simplicity. The supraorbital and supratrochlear nerves' trajectory cannot be distinguished from the MRI images because of having small diameters (which foramen of mentioned nerves are smaller than 1 mm, hence is assumed to be 1 mm in this study). Thus, these nerve volume models were extracted from the University College London library database which is called *ANATOMY.TV* (powered by primal pictures) and based on available anatomical data [18], [21].

2.3 Electrode Model

A gel patch was designed to cover the forehead due to the lower conductivity of the skin. The height of the gel patch was designed to be 35 mm and the length is 50 mm whilst the thickness was 1 mm (half of the patch thickness is pushed in the forehead skin layer to encourage appropriate simulation). An electrode matrix (8 × 4) was generated based on the forehead as shown in Fig. 3. The electrodes were spaced 10 mm vertically and 7 mm horizontally as shown in Fig. 3(c). It is not possible to decide which electrode arrangement results in better performance. Thus, all possible electrode configuration results were investigated by following the procedure. On the vertical axis for the first row, the first electrode was used as an *anode*, then the second one was used *cathode*. Then, the *anode* recording simulation position was kept constant, which is electrode 1 (E1) and the *cathode* electrode position was shifted at the horizontal axis until the E8 as detailed in matrix A and Fig. 3(c). The same procedure was applied to all rows. Then, E1 was defined *anode* and E9 was defined *cathode* then the *cathode* was shifted on the vertical axis. The same method was applied to all columns in the matrix A and Fig. 3(c). This resulted in 67 different electrode simulation configurations.

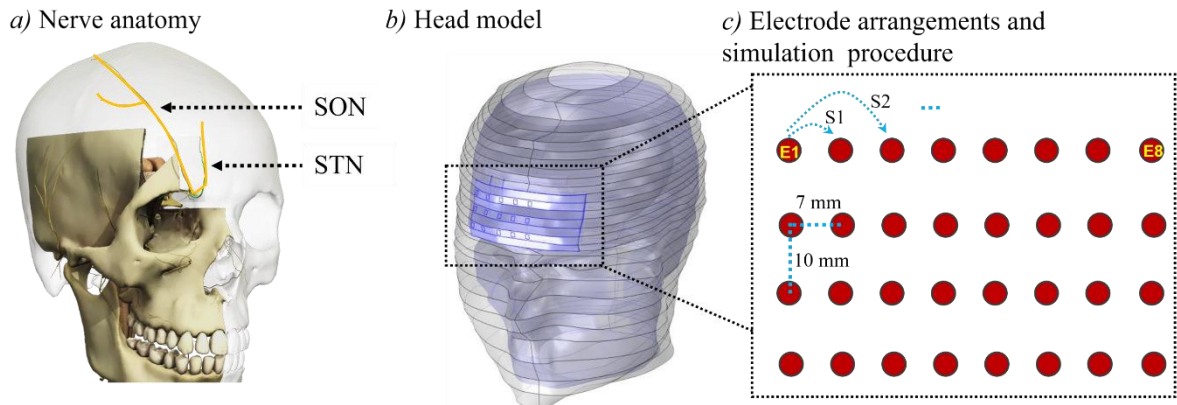


Figure 3. (a) Shows the anatomy of target nerve branches which are STN and SON, (b) Shows the 3D volume conductor of the human head that was generated in COMSOL. (c) Shows a schematic representation of electrode arrangements over the forehead of the human. The model was discretized and simulated to calculate electrical potential distribution within each domain. S1 represents simulation

1.

$$A = \begin{bmatrix} E1 & \dots & E8 \\ \vdots & \ddots & \vdots \\ E17 & \dots & E24 \end{bmatrix}$$

The electrodes are defined as equipotential surfaces where the electric current was conducted to the volume conductor of the human head model. In the current study, rectangular series of electrodes were placed on the patch. Each of the electrodes was designed to be in contact with the skin layer. In the COMSOL, *Terminal 1* was adjusted as an anode, and the current level of 1 mA was assigned in all cases. While *Terminal 2* was adjusted as cathode and -1 mA current level was applied. The air domain is set to ground (these cases are applied in all bipolar electrode configurations). The voltage simulation results are recorded for both STN and SON nerve fibers. This process was applied for 67 different bipolar electrode configurations for each nerve trajectory to estimate the optimal nerve activation location.

2.4 Finite Element Simulation

After generating a realistic volume of the human head model, the FEM process was performed to compute electric potential distributions along the neural tissue layer and the layers in the vicinity as shown in Fig.3. This electrical voltage distribution was generated by injecting current through electrode configuration. A sphere with a large diameter was defined around the model and the *Dirichlet boundary condition* ($V = 0$) was applied to the external boundaries of the sphere to obtain an accurate solution. This approximates ground condition at infinity. Additionally, external current density and the current source were set to zero everywhere in the model and the domains were discretized with *tetrahedral finite elements* to divide the model into small geometrical shapes. Whilst skin, muscle, electrode patch, and nerves finely meshed; brain, skull, and air layers were coarser meshed. This resulted in approximately 6.2 million elements (about 7.7 million degrees of freedom). After adjusting the optimum sphere radius and optimum meshing quality, the simulation results were obtained by means of quasi-static approximation of Maxwell Equations in COMSOL that can be expressed through Laplace formulation, as shown in (1).

$$\nabla \cdot ([\sigma] \nabla V) = 0 \quad (1)$$

where σ is the conductivity of each of the tissue layers; V is the electrical potential in representing geometry. The electrical potential distributions within the volume conductor were calculated by applying the dielectric parameter of the associated layers. These tissues' dielectric properties are depicted in Table 1. To highlight, the sphere (air) domain conductivity was set to $(1e-10)$ S/m, whilst gel conductivity, gel

relative permittivity, and air relative permittivity are all set to 1 to obtain a unique solution in COMSOL. It is noted that the tissue dielectric parameters were suited based on low frequency (10 Hz).

Table 1. Tissue conductivity.

Tissue layers	Conductivity [S/m]	Reference
Skin	2.00e-4	[25]
Nerve	1.71e-2	[26]
Muscle	2.02e-1	[27]
Skull	2.00e-2	[28]
Brain	4.75e-2	[25]
Gel	1	
Air	1e-10	

After adjusting the conductivity of different domains in the model, the radius of the external sphere was changed from 40 cm to 300 cm in steps and the resulting simulation of the electric potential along the trajectory of the nerve was recorded. These results were simulated and indicated only a shift in the electrical potential along the nerve fiber. There was less than a 3 % variation in voltage results across the nerve for an external sphere radius between 60 cm to 300 cm. Thus, the external sphere radius was set at 60 cm for the rest of the study due to low computational time.

2.5 Nerve Model

Myelinated fiber diameter was obtained from [22] as 12 μm with a standard deviation of 2 μm in MATLAB to generate fiber diameter distribution. The node of Ranvier was randomly placed between 0 and Δx (node-to-node distance for the mentioned nerve diameter) along the arc length of the said nerve. The geometric parameters of passive compartments were generated by linear interpolation based on fiber diameter. These passive compartments were placed in sequence along the arc length of nerve and fiber completed by a node. These processes were iterated 100 times for approximately 3.6 cm nerve trajectory. The electrical potential along the nerve was calculated in COMSOL for each electrode configuration. This step was repeated for each nerve potential distribution.

2.6 Activation Function (AF)

The AF is a powerful tool used to obtain a view along the given nerve with possible positions of depolarization and hyperpolarization. More precisely, Rattay et al. [23] have introduced the AF as a second spatial derivative of the extracellular voltage which is shown in (2). This simplistic calculation provides to predict action potential generation. The voltage which was generated in COMSOL referred to as extracellular voltage was applied in MATLAB to generate the AF.

$$AF = \frac{\Delta^2 V_e}{\Delta l^2} = \frac{V_e(n-1) - 2V_e(n) + V_e(n+1)}{\Delta x^2} \quad (2)$$

$V_{e(n)}$ = extracellular potential on the nth node of the myelinated fiber

l = arc-length of the nerve

Δx = node to node distance

AF distributions were generated in MATLAB for 100 axons randomly placed along both STN and SON nerve trajectories with the normal distribution of fibre diameter for all the possible bipolar electrode configurations. The extracellular voltage that was generated in FEM is multiplied by -1 to get AF distribution for reverse electrode configuration. The same process was repeated for all nerve trajectories.

3. RESULTS

3.1 Electrical Potential Variation

The electrical potential distributions across the different nerve fibers of STN and SON based on different electrode arrangements for different polarities of the current are shown in Fig. 4, and Fig. 5, respectively. Since the AF is the main finding of this study, the electrical potential distribution across the nerve fiber for the electrode configuration is shown for two samples.

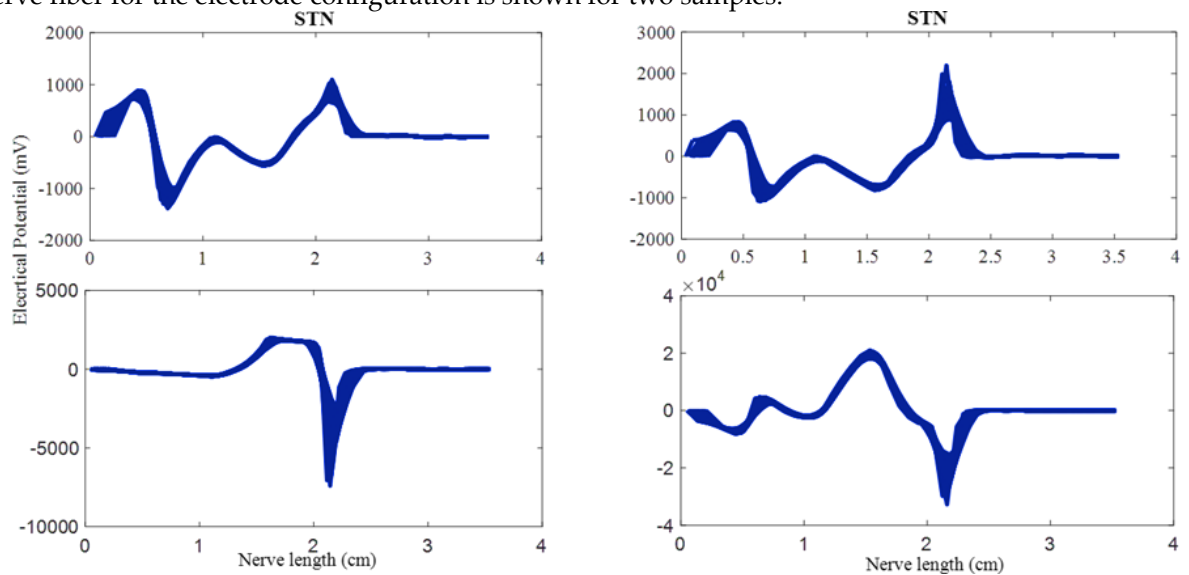


Figure 4. Electrical potential distributions across the STN nerve fibers for different electrode arrangements using both positive and negative values of the same current levels.

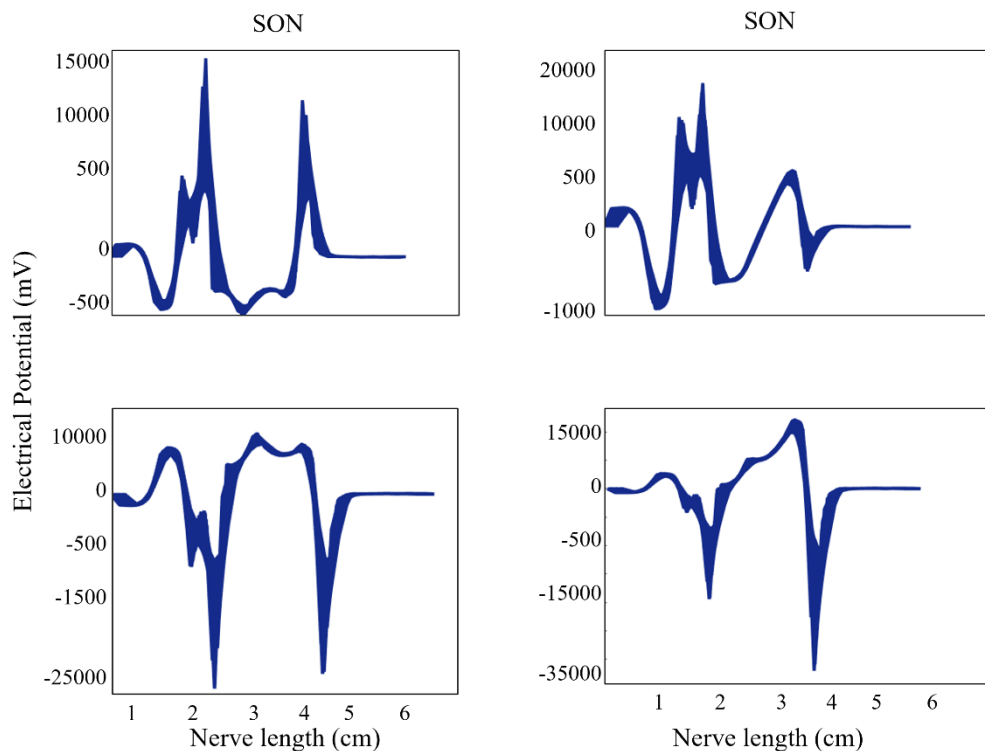


Figure 5. Electrical potential distributions across the SON nerve fibers for different electrode arrangements using both positive and negative values of the same current levels.

It is clearly shown that the extracellular potential distributions along the nerve fibers are various for the given electrode settings. The anodic and cathodic stimulation shows different electrical potential variations based on given neuromodulator settings. The recorded electrical potential range for the anodic stimulation is about -2 V to 3 V. This range is about -40 V to 40 V for cathodic stimulation. It is noted that the sharp variation in the electric potential variations is recorded approximately at the same location of the nerve fibers for the STN and SON nerves based on both anodic and cathodic stimulations. Although the electrical potential variation for the nerve fibers varies, this is not a significant variation (≈ 1 mV) to affect the outcome of the action potential generation position as all nerve fibers show the same electrical potential trend versus the arc length is similar.

3.2. Action Potential Based on AF

The AF variation versus the nerve length for both STN and SON nerve branches is shown in Fig. 5. The AF variation for both cathodic and anodic stimulation of SON and STN nerve fibers are shown in Fig. 6(a), and (b), respectively. The AP results for different nerve fibers are highlighted.

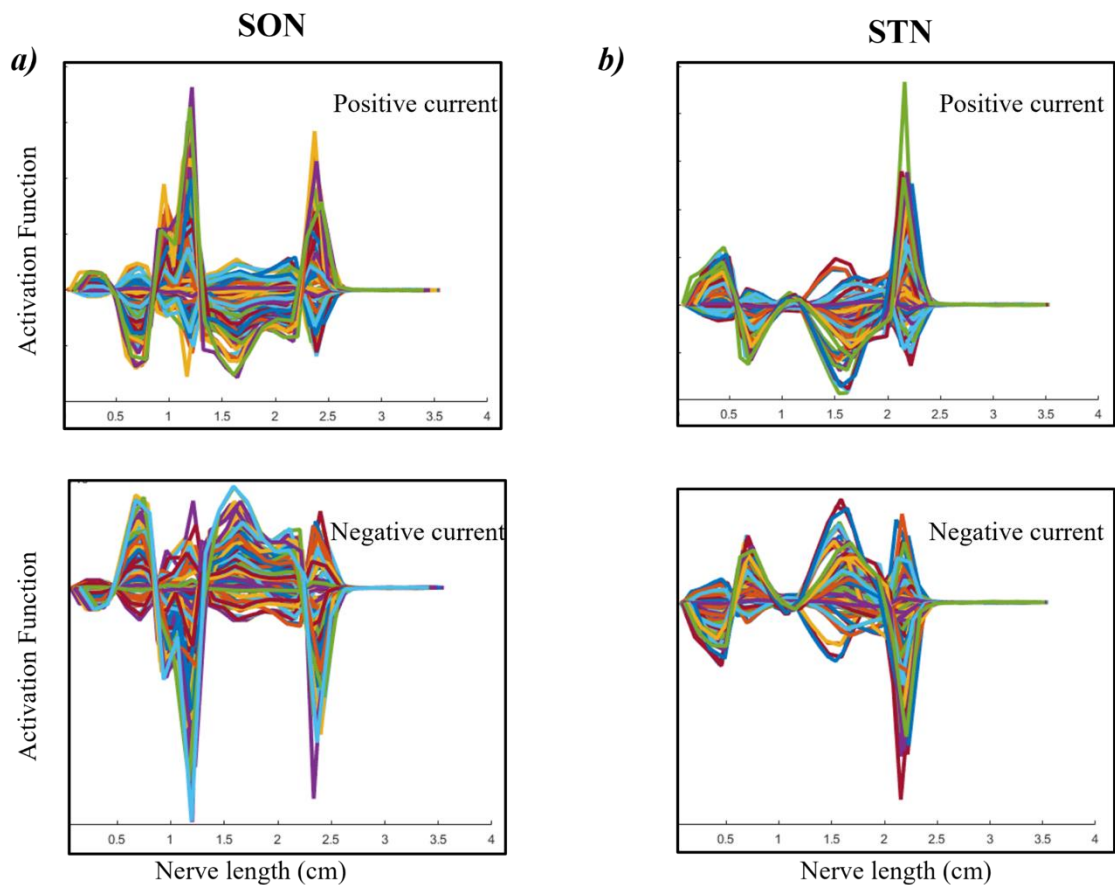


Figure 6. (a) Shows AF versus nerve length for SON nerve fibers based on different current polarities. (b) Shows AF versus nerve length for STN nerve fibers based on different current polarities.

It is shown that the maximum positive and maximum negative values of the AF are nearly observed at the same place of the nerve length for both SON and STN nerves. The SON may be activated at the places along the nerve trajectory as there are two sudden changes in the AF. For STN, the nerve fibres can be activated only in a region of the nerve trajectory. When the AF is positive, that means the nerve can be activated. As can be seen from Fig. 4, Fig. 5, and Fig. 6, the AF varies for STN and SON nerves. The possibility of generating AP along the STN nerve is around 2.3 cm. Whilst, the depolarization possibility of the SON nerve can occur at two different places along the nerve (about 1.2 cm and 2.5 cm). It is noted

that although the electrical potential variation across the nerve fibers showed various patterns, the possible place of the action potential generation is the same for both SON and STN nerves.

4. DISCUSSION

TENS neuromodulation has a wide variety of applications in basic research, medical treatments, and the design of neuronal prostheses. The research of neural responses to electrical stimuli is focused on both invasive and non-invasive experiments. It may not be possible to investigate the exact location of the neural tissue activation due to the complexity of the experiments. Thus, the computational methods are used as an alternative which has a significant role in the interpretation of the experimental results, the prediction of the outcome of adapted experiments, and the translation of the experimental findings into possible technical strategies for treatments. The neural response to the electrical potential can be calculated using a multi-compartment model composed of the fundamental tissue layers by stimulating electrode arrangements [4], [5], [16], [17], [24]. In this study, an accurate multi-layered human head was developed based on MRI data to define the optimal location of the nerve fiber activation based on AF using such models. The volume conductor was simulated, and the results were recorded.

The electrical potential for STN based on different current and electrode arrangements was shown in Fig. 4. It was shown that although the electrical potential was significantly varied, the peak location of the electrical potential was about the same. This was valid for both anodic and cathodic stimulations. This may show the vicinity of functioning neurons. Thus, the generating action potentials can be triggered in the proximity of that region [16]. It was noted that the anodic stimulation showed at least two peak variations in the electrical potential for both electrode arrangement samples. This variation was only observed for a sample of cathodic stimulation. This can be associated with nerve fibers with cell bodies in proximity. These nerve fibers can be activated on lower thresholds using anodic stimulation [16].

The results in Fig. 6 suggested that the nerve fibers can be activated at the different locations of the nerve arc length for some samples. However, it was clear that AF was observed at a certain arc length of the nerve fibers (≈ 2.3 cm) for all samples. Thus, the results of this study suggested that the nerve fibers can be activated at this location of nerve fibers-based AF.

Also, it was suggested that it may not be possible to generate action potential along the nerve fibers, although the electrical potential variation was relatively higher. The magnitude of the electrical potential variation was higher for the second sample of the anodic stimulation as shown in Fig. 4. The nerve fibers were activated at two locations along the nerve fibers as shown in Fig. 6.

Although an accurate and multi-layered human head model was developed and appropriate boundary conditions were applied to generate possible activation locations, the study was constructed based on low frequency. Since the dielectric properties of the anatomical tissue vary, this may influence the outcome.

5. CONCLUSIONS

FEM modeling is commonly applied in many branches of biomedical engineering and basic research in neurosciences for both invasive and non-invasive applications. Thus, a multi-layered human head was generated based on accurate FEM-based computational models to investigate the possible and feasible location of the nerve fibers activation based on electrode configuration using dielectric properties of the anatomical tissue layers. The AF was used to predict the possible location of the action potential generation of the nerve fibers using such computational methods. The results showed that action potential can be generated at the location of the nerve trajectory that showed a sudden change in the extracellular electrical potential. Also, it was suggested that the electrode proximity to the neural tissue may influence the outcome. It was noted that the magnitude of the extracellular electrical potential was not always proportional to AF.

REFERENCES

- [1] N. Ravichandran, M. Y. Teo, K. Aw, and A. McDaid, "Design of Transcutaneous Stimulation Electrodes for Wearable Neuroprostheses," *IEEE Transactions on Neural Systems and Rehabilitation Engineering*, vol. 28, no. 7, pp. 1651–1660, Jul. 2020, doi: 10.1109/TNSRE.2020.2994900.
- [2] B. A. Karamian *et al.*, "The role of electrical stimulation for rehabilitation and regeneration after spinal cord injury," *Journal of Orthopaedics and Traumatology*, vol. 23, no. 1. Springer Science and Business Media Deutschland GmbH, Dec. 01, 2022. doi: 10.1186/s10195-021-00623-6.
- [3] A. Gupta, N. Vardalakis, and F. B. Wagner, "Neuroprosthetics: from sensorimotor to cognitive disorders," *Communications biology*, vol. 6, no. 1. NLM (Medline), p. 14, Dec. 01, 2023. doi: 10.1038/s42003-022-04390-w.
- [4] E. Salkim, A. Shiraz, and A. Demosthenous, "Impact of neuroanatomical variations and electrode orientation on stimulus current in a device for migraine: A computational study," *J Neural Eng*, vol. 17, no. 1, 2020, doi: 10.1088/1741-2552/ab3d94.
- [5] E. Salkim, A. Shiraz, and A. Demosthenous, "Influence of cellular structures of skin on fiber activation thresholds and computation cost In fl uence of cellular structures of skin on fi ber activation thresholds and computation cost," *Biomed Phys Eng Express*, vol. 5, no. 1, p. 015015, 2018.
- [6] S. Joucla, A. Glière, and B. Yvert, "Current approaches to model extracellular electrical neural microstimulation," *Front Comput Neurosci*, vol. 8, no. February, pp. 1–12, 2014, doi: 10.3389/fncom.2014.00013.
- [7] S. F. Cogan, "Neural Stimulation and Recording Electrodes," *Annu Rev Biomed Eng*, vol. 10, no. 1, pp. 275–309, 2008, doi: 10.1146/annurev.bioeng.10.061807.160518.
- [8] A. Kuhn, T. Keller, M. Lawrence, and M. Morari, "The influence of electrode size on selectivity and comfort in transcutaneous electrical stimulation of the forearm," *IEEE Transactions on Neural Systems and Rehabilitation Engineering*, vol. 18, no. 3, pp. 255–262, Jun. 2010, doi: 10.1109/TNSRE.2009.2039807.
- [9] A. Patriciu, K. Yoshida, J. J. Struijk, T. P. DeMonte, M. L. G. Joy, and H. Stødkilde-Jørgensen, "Current density imaging and electrically induced skin burns under surface electrodes," *IEEE Trans Biomed Eng*, vol. 52, no. 12, pp. 2024–2031, Dec. 2005, doi: 10.1109/TBME.2005.857677.
- [10] D. Magis, S. Sava, T. S. d'Elia, R. Baschi, and J. Schoenen, "Safety and patients' satisfaction of transcutaneous supraorbital neurostimulation (tSNS) with the Cefaly® device in headache treatment: a survey of 2,313 headache sufferers in the general population.," *J Headache Pain*, vol. 14, p. 95, 2013, doi: 10.1186/1129-2377-14-95.
- [11] J. Schoenen *et al.*, "Migraine prevention with a supraorbital transcutaneous stimulator: A randomized controlled trial," *Neurology*, vol. 80, no. 8, pp. 697–704, 2013, doi: 10.1212/WNL.0b013e3182825055.
- [12] E. Salkim, "Electrode Array Position Guiding in Cochlea Based on Impedance Variation : Computational Study," *Muş Alparslan Üniversitesi Mühendislik Mimarlık Fakültesi Dergisi*, vol. 1, no. 1, pp. 64–71, 2020.
- [13] A. Fellner, A. Heshmat, P. Werginz, and F. Rattay, "A finite element method framework to model extracellular neural stimulation," *J Neural Eng*, vol. 19, no. 2, Apr. 2022, doi: 10.1088/1741-2552/ac6060.
- [14] F. Rattay, S. M. Danner, U. S. Hofstoetter, and K. Minassian, "Finite Element Modeling for Extracellular Stimulation," in *Encyclopedia of Computational Neuroscience*, Springer New York, 2014, pp. 1–12. doi: 10.1007/978-1-4614-7320-6_593-5.
- [15] S. Joucla and B. Yvert, "Modeling extracellular electrical neural stimulation: From basic understanding to MEA-based applications," *Journal of Physiology-Paris*, vol. 106, no. 3–4, pp. 146–158, 2012, doi: 10.1016/j.jphysparis.2011.10.003.

- [16] H. Ye, "Finding the Location of Axonal Activation by a Miniature Magnetic Coil," *Front Comput Neurosci*, vol. 16, Jun. 2022, doi: 10.3389/fncom.2022.932615.
- [17] D. N. Anderson, G. Duffley, J. Vorwerk, A. D. Dorval, and C. R. Butson, "Anodic stimulation misunderstood: Preferential activation of fiber orientations with anodic waveforms in deep brain stimulation," *J Neural Eng*, vol. 16, no. 1, Feb. 2019, doi: 10.1088/1741-2552/aae590.
- [18] K. N. Christensen, N. Lachman, W. Pawlina, and C. L. Baum, "Cutaneous Depth of the Supraorbital Nerve," *Dermatologic Surgery*, vol. 40, no. 12, pp. 1342–1348, 2014, doi: 10.1097/DSS.000000000000174.
- [19] Y.-C. Gil, K.-J. Shin, S.-H. Lee, W.-C. Song, K.-S. Koh, and H. J. Shin, "Topography of the supraorbital nerve with reference to the lacrimal caruncle: danger zone for direct browplasty," *British Journal of Ophthalmology*, vol. 101, no. 7, pp. 940–945, 2017, doi: 10.1136/bjophthalmol-2016-309332.
- [20] "OVERVIEW » IT'IS Foundation." <https://itis.swiss/virtual-population/regional-human-models/overview/> (accessed Jan. 20, 2023).
- [21] A. K. D. Harold Ellis, Bari M Logan, *Human Sectional Anatomy*, Third Edit. London: Hodder Arnold, 2009.
- [22] M. Z. Siemionow, "The Face as a Sensory Organ," in *The Know-How of Face Transplantation*, M. Siemionow, Ed., Springer, 2011, pp. 207–212. doi: 10.1007/978-0-85729-253-7.
- [23] F. Rattay, "Analysis of models for extracellular fiber stimulation.pdf," *IEEE Trans. Biomed. Eng.*, vol. 36, no. 7, pp. 676–682, 1989.
- [24] A. Fellner, A. Heshmat, P. Werginz, and F. Rattay, "A finite element method framework to model extracellular neural stimulation," *J Neural Eng*, vol. 19, no. 2, Apr. 2022, doi: 10.1088/1741-2552/ac6060.
- [25] "Low Frequency (Conductivity) » IT'IS Foundation." <https://itis.swiss/virtual-population/tissue-properties/database/low-frequency-conductivity/> (accessed May 20, 2019).
- [26] E. Salkim, "Optimisation of a Wearable Neuromodulator for Migraine Using Computational Methods."
- [27] E. Salkim, "Analysis of tissue electrical properties on bio-impedance variation of upper limbs", doi: 10.3906/elk-1300-0632.3908.
- [28] T. F. Oostendorp, J. Delbeke, and D. F. Stegeman, "The conductivity of the human skull: Results of in vivo and in vitro measurements," *IEEE Trans Biomed Eng*, vol. 47, no. 11, pp. 1487–1492, Nov. 2000, doi: 10.1109/TBME.2000.880100.